RASIM: A Novel Rotation and Scale Invariant Matching of Local Image Interest Points

Mahdi Amiri and Hamid R. Rabiee, *Senior Member, IEEE*

***Abstract*—This paper presents a novel algorithm for matching image interest points. Potential interest points are identified by searching for local peaks in Difference-of-Gaussian (DoG) images. We refine and assign rotation, scale and location for each keypoint by using the SIFT algorithm [1]. Pseudo log-polar sampling grid is then applied to properly scaled image patches around each keypoint, and a weighted adaptive lifting scheme transform is designed for each ring of the log-polar grid. The designed adaptive transform for a ring in the reference keypoint and the general non-adaptive transform are applied to the corresponding ring in a test keypoint. Similarity measure is calculated by comparing the corresponding transform domain coefficients of the adaptive and non-adaptive transforms. We refer to the proposed versatile system of *Rotation And Scale Invariant Matching* as *RASIM*. Our experiments show that the accuracy of RASIM is more than SIFT, which is the most widely used interest point matching algorithm in the literature. RASIM is also more robust to image deformations while its computation time is comparable to SIFT.**

***Index Terms*—Adaptive lifting scheme, object detection, rotation/scale invariant template matching.**

I. Introduction

TEMPLATE matching is extensively used in applications such as video surveillance [2], autonomous navigation [3], object-based coding [4], visual control [5], image registration [6], [7], image recognition [8], object detection [9], stereo matching [10], and image retrieval systems [11], [12].

Invariance to scale and rotation and ability to handle partial occlusion are among the most desired robustness properties in the field of template matching. We have provided a brief survey of the recent rotation/scale invariant template matching algorithms in [13]. In the same reference, we introduced a novel rotation and scale invariant template matching algorithm based on adaptive lifting scheme that used a combination of small number of template views, called vertex templates; however, it was not able to handle partial occlusion.

More recently, interest point based algorithms for template matching applications have received considerable attention within the image understanding community. In particular, they are resistant to partial occlusion, are relatively insensitive to changes in viewpoint and can be computed efficiently [14]. It has been shown that the accuracy ranking of different algorithms is relatively insensitive to the method employed to find interest points in the image but it is dependent on the representation used to model the image patch around the interest points [14], [15].

In this paper, we find the interest points by using the SIFT algorithm [1], but to model the image patch around the interest points, we will use a pseudo log-polar sampling grid on the properly scaled image patches around each keypoint, instead of the commonly used Cartesian grid. The contents of each ring in the log-polar grid will be used to create a data vector for each ring. For any given reference data vector, we employ a novel algorithm to design an adaptive lifted wavelet transform. At the matching stage, both of the designed adaptive lifted wavelet transform and the general non-adaptive wavelet transform are applied to any given test data vector. Similarity measure between the reference data vector and the test data vector is calculated by comparing the corresponding transform domain coefficients of adaptive and non-adaptive transforms.

The rest of this paper is organized as follows. Section II will provide a survey of the recent rotation/scale invariant template matching algorithms and adaptive wavelet transforms. The proposed detection algorithm is described in Section III and the experimental results are presented in Section IV. Finally, the future work to further improve the performance of the proposed algorithm and the concluding remarks are presented in Section V.

II. Related Works

In 1999, David Lowe published a paper describing a novel method called SIFT, for extracting distinctive invariant features from images that can be used to perform reliable matching between different views of an object or scene [16]. Soon after, the idea of representing local image features by histograms of gradient locations and orientations became a widely accepted approach for image matching algorithms.

Many attempts to improve the SIFT have been presented during the past decade. Bay *et al.* proposed SURF [17] as an efficient implementation of SIFT by relying on integral images to compute image convolutions and using a small number of histogram bins for quantizing the gradient orientations. Agrawal *et al.* proposed CenSurE [18] in which features are computed at the extrema of the center-surround filters over multiple scales. Center surround extremas can be computed in real time using integral images. These were just two prominent examples of many other modified versions of SIFT, which have been reported in the literature [19]. Most of the modified versions try to achieve better computational characteristics.

Manuscript received February 18, 2010; revised October 01, 2010, February 23, 2011, and April 25, 2011; accepted May 07, 2011. Date of publication May 19, 2011; date of current version November 18, 2011. The associate editor coordinating the review of this manuscript and approving it for publication was Dr. Arun Ross.

The authors are with the AICTC Research Center, Department of Computer Engineering, Sharif University of Technology, Tehran 1478619338, Iran (e-mail: m_amiri@ce.sharif.edu; rabiee@sharif.edu).

Color versions of one or more of the figures in this paper are available online at http://ieeexplore.ieee.org.

Digital Object Identifier 10.1109/TIP.2011.2156800

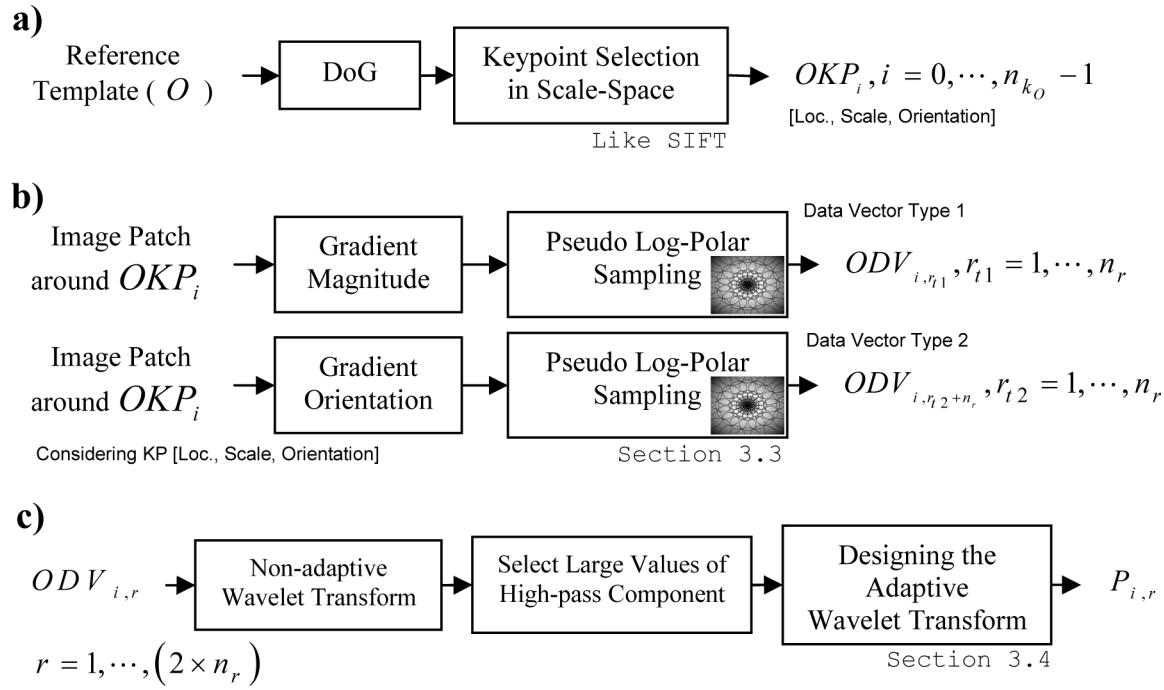

Fig. 1. Block diagram of RASIM, Offline step. (a) Finding keypoints of the reference template, (b) Preparing data vectors of reference image patch around each keypoint, (c) Designing the adaptive wavelet transform for each data vector.

Although they are more efficient than the original SIFT for some test images with specific degradations, but in general they perform worse than SIFT in terms of quality of matching. So far, no interest point method have been capable to outperform SIFT in a wide range of applications.

We have already developed object detection algorithms based on the adaptive lifting scheme to provide different robustness properties [13], [20]. The basic detection algorithm along with the ability to adapt to uncertainty about object properties, ability to adapt to the changing local image statistics, ability to adapt to high background noise and slight deformations in the object of interest are presented in [20], and the rotation/scale invariance properties were included in the detection algorithm of [13]. While the algorithm in [13] had acceptable results for the slight deformations in the object of interest, but it was not resistant to partial occlusion.

In this paper, we introduce a new adaptive lifting scheme based detection algorithm that can be applied to the image patches around specific interest points. We refer to the proposed algorithm as RASIM which stands for "Rotation And Scale Invariant Matching". The proposed algorithm has a completely different approach for object detection compared to our previous work in [13], here we use interest points, while in [13] we were using the combination of a small number of template views, called vertex templates. By using interest points, we may also achieve resistance to partial occlusion and relative insensitivity to changes in the viewpoint, besides preserving robustness properties of our previous works.

III. The Proposed Detection Algorithm

The block diagram of RASIM is shown in Fig. 1 (offline step) and Fig. 2 (online step). In this section, we first describe the main building blocks of each diagram, individually. Then the role of each building block in the whole detection system will be discussed.

A. Problem Definition

Consider a $m \times n$ reference template O and an $M \times N$ input test image T. The problem of template matching can be stated as follows: To find the rotation angle θ, the scale factor α and location (u, v) in the image T that minimizes the objective function

$$\arg\max_{u,v,\theta,\alpha} f(u, v, \alpha \otimes (\theta \odot T)) \tag{1}$$

where $\odot$ denotes the rotation operator and $\otimes$ denotes the scale operator. The function f is a measure of similarity between the rotated and scaled template $O' = \alpha \otimes (\theta \odot T)$ and the image patch T' from image T centered at (u, v). Different matching methods take different forms of function f. As a classic example, f may represent the normalized cross correlation.

B. Keypoint Selection

The standard SIFT keypoint selection process as described in [16] already poses an efficient and carefully designed refining method. On the other hand, it has been shown that between "interest point selection method" and "the representation method used to model the image patch around the interest point", the latter one has much more effect in the ranking of accuracy for different algorithms [14]. Therefore, in this paper we select the keypoints similar to the SIFT algorithm, but later will use a new model for the image patch around the interest points based on the pseudo log-polar sampling grid.

The potential interest points are identified by searching for maxima and minima in the scale-space representation of an image. This scale-space representation is produced by the Difference-of-Gaussian (DoG) images. A few other refining

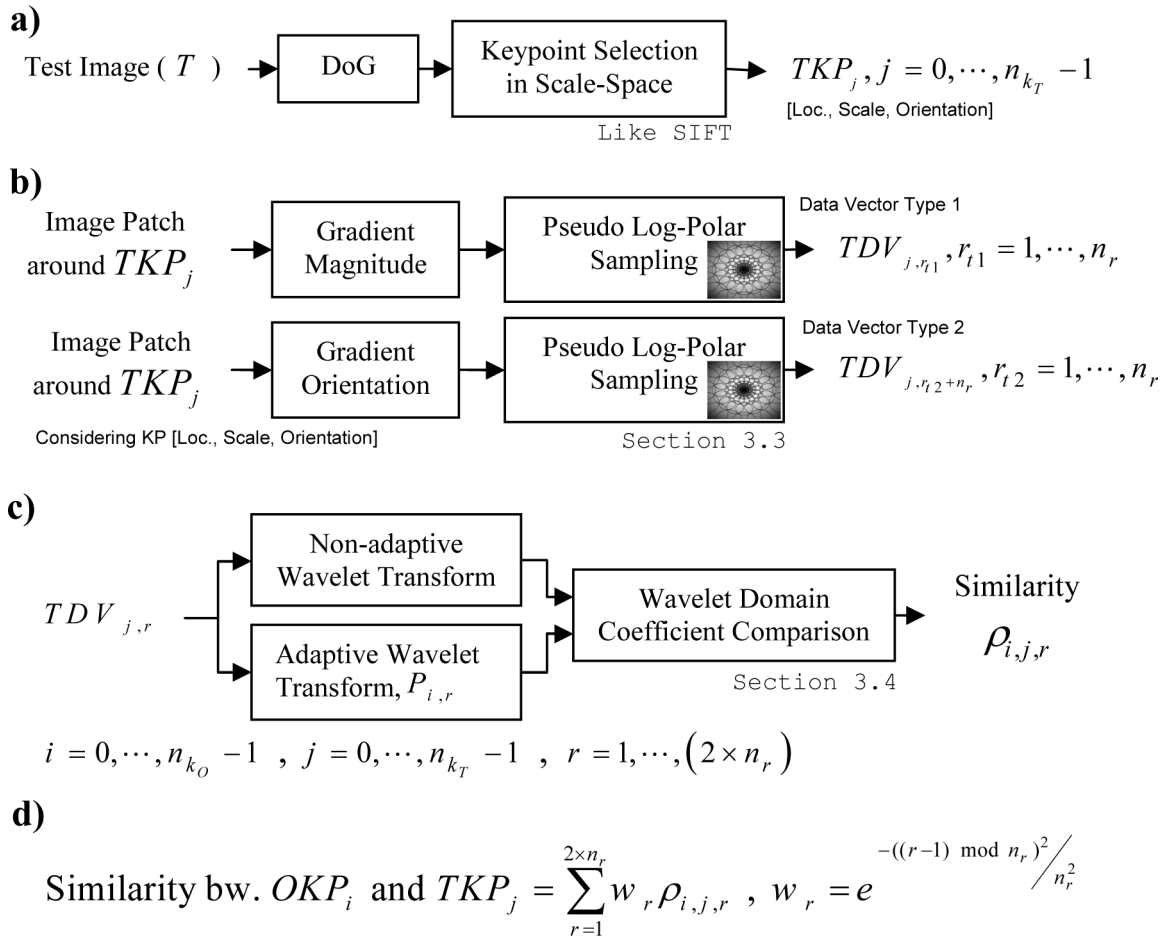

Fig. 2. Block diagram of RASIM, Online step. (a) Finding keypoints of the test image, (b) Preparing data vectors of test image patch around each keypoint, (c) Computing similarity between reference template and test image data vectors using the designed adaptive wavelet, (d) Computing similarity between keypoint pairs as weighted sum of similarity between their data vectors.

and eliminating stages are applied in the SIFT algorithm to assign proper orientation, scale and location for each keypoint. In RASIM, we employ this keypoint selection process in the offline step for finding the reference object template keypoints (OKPs) as illustrated in Fig. 1(a), and in the online step for finding the test image keypoints (TKPs) as shown in Fig. 2(a).

C. Preparing Data Vectors

Before going through the core of matching algorithm based on the adaptive wavelet transform, we convert the image patches around each keypoint to a set of data vectors. First we employ the gradient magnitude and gradient orientation of the subimage around each keypoint as two different input data types. The structure of RASIM could simply incorporate more than two different input data types, when more robustness is required and we have enough free processing time.

Then, we apply a pseudo log-polar mapping on each subimage, instead of passing the common Cartesian image pixel values to the next step. The log-polar mapping inherently includes both ring and radial projections. This property will mostly enhance the results of the matching algorithm when the assigned rotation and scale for the keypoints are slightly degraded. This is because we chose the log-polar pixels of each ring as a separate input data vector (DV) for the matching algorithm.

There is a vast amount of literature related to the fields of template matching, image registration and motion estimation that make use of log-polar mapping based methods. The motivations in this regard stem from its scale and rotation invariance properties and the existence of a biological foundation. The pseudo log-polar sampling grid with different number of rings, n_r and number of receptive fields (circles) in each ring, n_θ is illustrated in Fig. 3.

The main geometric properties and a well-accepted mathematical definition for the projection of the retina onto the human visual cortex are presented by Schwartz [21]. His model has only theoretical significance and due to singularity of the logarithmic function in the origin (fovea), it cannot directly be used for a computer implementation. To avoid the problem of having infinite mapping in the fovea, different solutions have been proposed. A good study of the existing log-polar mapping models and their properties may be found in [22].

We have chosen the model of Tistarelli-Sandini [23] for the log-polar mapping as it presents both rotation and scale invariance properties [13]. Although this model will include blindness in fovea, but the blind area is not extended more than a few pixels and could be ignored.

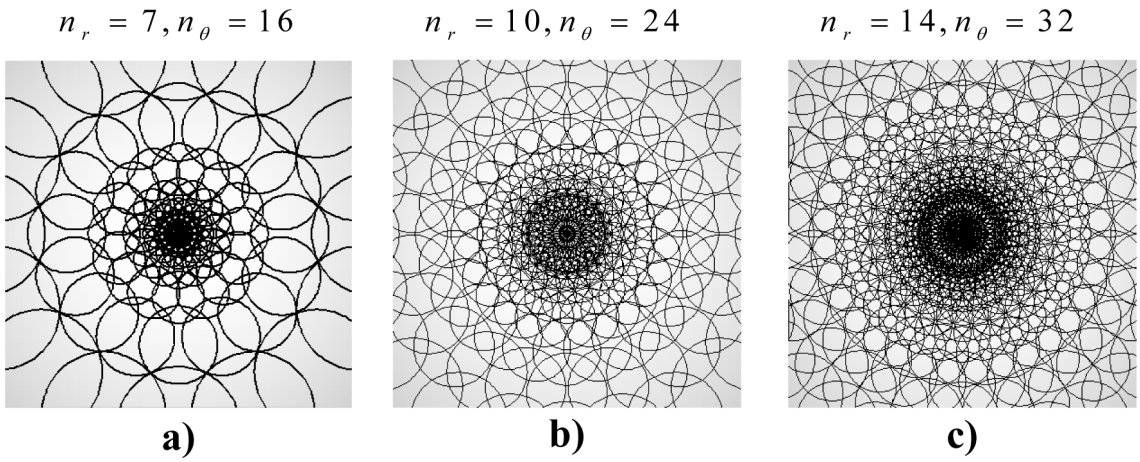

Fig. 3. Pseudo log-polar sampling grid with different number of rings, n_r and number of receptive fields (circles) in each ring, n_θ.

We perform log-polar mapping in software by the lookup table (LUT) method. Every log-polar pixel (ξ, η) will be calculated by the normalized weighted sum of a list of Cartesian pixels (x, y). A fast algorithm for generating this LUT is presented in [22]. At the offline step we initialize such a list for each log-polar pixel in the LUT. Therefore, it will be used wherever in the object detection system that the log-polar mapping is required.

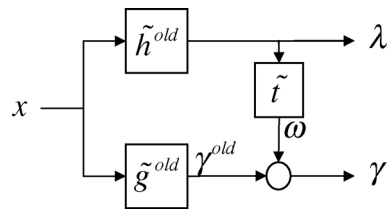

Fig. 4. Fast lifted wavelet transform using dual lifting step.

D. Designing the Adaptive Wavelet Transform

Designing an adaptive wavelet transform for a given data vector based on the lifting scheme structure is the main building block of RASIM. First the classical wavelet transform is applied to the given data vector and large values in the high-pass component of this non-adaptive wavelet transform are considered to be the data features. The main idea of the proposed detection algorithm is the design of an adaptive transform based on these features. Therefore, our new adaptive wavelet transform is designed such that the desired large coefficients in the high-pass component of the non-adaptive transform vanish in the high-pass component of the adaptive transform.

The process of vanishing data features in the transform domain will help us in two ways. First, it will assist us to construct a system of linear equations for designing the desired adaptive wavelet transform as described in Section III.D.2. Second, it will provide a basis for comparing the outcome of the adaptive and non-adaptive filters which is the essence of similarity measurement in our matching system. In the online step, we apply both non-adaptive and adaptive transforms to a given test data vector. Then, the high-pass component coefficients of the non-adaptive and the adaptive wavelet transforms are compared for calculating the similarity value.

In the following subsections, we first introduce the concept of dual lifting step in the lifting scheme. Then, it will be shown that how we could design the desired adaptive wavelet transform for a reference object data vector (ODV) using the lifting scheme structure. Although the design of adaptive wavelet transform for 1-D signals have already been presented in [13]; for the proposed algorithm the *1-D input signal* is replaced with *reference object data vector (ODV)* and the *1-D test signal* is replaced with *test data vector (TDV)*. Therefore, we have repeated the derivation steps in the following subsections to keep this paper as self contained. This is followed by introduction of the algorithm for finding the similarity measurement between a reference data vector and a test data vector (TDV). Finally, we provide a discussion on selection of the required parameters of this algorithm and its efficiency. Moreover, a weighted adaptive version of the proposed similarity measurement method will be presented that enhances the detection power of our algorithm [24].

1) The Dual Lifting Step: The fast lifted wavelet transform block diagram using a dual lifting step [25] is shown in Fig. 4. Here, $\tilde{h}^{\text{old}}$ and $\tilde{g}^{\text{old}}$ are the low-pass and high-pass analysis filters of the non-adaptive wavelet transform that are applied to the input signal x, respectively. The prediction filter $\tilde{t}$ is applied to the low-pass component λ and the output ω is subtracted from the old high-pass component, γ^{old}, in order to produce the new high-pass component γ as follows:

$$\omega = (x * \tilde{h}^{\text{old}}) * \tilde{t} \tag{2}$$

$$\gamma^{\text{old}} = x * \tilde{g}^{\text{old}} \tag{3}$$

$$\gamma = \gamma^{\text{old}} - \omega \tag{4}$$

where $*$ denotes the convolution operator.

2) The Prediction Filter: In this subsection, we show how to find the coefficients of the prediction filter $\tilde{t}$, such that the coefficients of the non-adaptive wavelet transform's high-pass component, vanish in the high-pass component of the adaptive lifted wavelet transform. Let s be the signal of interest (a reference

object data vector, ODV, in RASIM). Applying the non-adaptive wavelet transform to this signal will produce the following low-pass (λ) and high-pass (γ^{old}) components

$$\lambda = s * \tilde{h}^{\text{old}} \Rightarrow \lambda_k = \sum_j s_j \tilde{h}^{\text{old}}_{k+1-j} \tag{5}$$

$$\gamma^{\text{old}} = s * \tilde{g}^{\text{old}} \Rightarrow \gamma^{\text{old}}_k = \sum_j s_j \tilde{g}^{\text{old}}_{k+1-j} \tag{6}$$

where k is the index of elements belonging to low-pass and high-pass components and j is the index of elements belonging to the source signal s.

Given the prediction filter $\tilde{t}$, the high pass component of the adaptive lifted wavelet transform (γ) is obtained as follows:

$$\omega = \lambda * \tilde{t} \Rightarrow \omega_k = \sum_j \lambda_j \tilde{t}_{k+1-j} \tag{7}$$

$$\gamma_k = \gamma^{\text{old}}_k - \omega_k. \tag{8}$$

If we consider a coefficient in the old high-pass component γ^{old}, with index k', which has a relatively large magnitude and try to vanish its corresponding coefficient in the high-pass component γ, based on (8), we would have

$$\gamma_{k'} = 0 \Rightarrow \omega_{k'} = \gamma^{\text{old}}_{k'} \tag{9}$$

and by substituting ω from (7), we obtain

$$\sum_j \lambda_j \tilde{t}_{k'+1-j} = \gamma^{\text{old}}_{k'}. \tag{10}$$

On the other hand, it is known that, the high-pass analysis filter for the adaptive lifted wavelet transform is given by the following equation [25]

$$\tilde{g}^{\text{new}}(z) = \tilde{g}^{\text{old}}(z) + \tilde{h}^{\text{old}}(z)\tilde{t}(z^2). \tag{11}$$

Clearly, the summation of the filter coefficients is equal to zero

$$\sum_k \tilde{g}^{\text{new}}_k = 0 \tag{12}$$

which is equivalent to:

$$\sum_k \tilde{t}_k = 0. \tag{13}$$

Let p be the length of the prediction filter $\tilde{t}$. Now if we let v be the number of selected large coefficients of the old high-pass component with indices $k'_1, k'_2, \ldots, k'_v$, we would have

$$\left|\gamma_{k'_1}\right| > \left|\gamma_{k'_2}\right| \cdots > \left|\gamma_{k'_v}\right| \tag{14}$$

and then we try to vanish their corresponding coefficients in the new high-pass component. Considering (10) and (13), a linear system of equations could be formed as (15)

$$\begin{bmatrix} \lambda_{k'_1} & \lambda_{k'_1-1} & \cdots & \lambda_{k'_1-p+1} \\ \lambda_{k'_2} & \lambda_{k'_2-1} & \cdots & \lambda_{k'_2-p+1} \\ \vdots & \vdots & \ddots & \cdots \\ \lambda_{k'_v} & \lambda_{k'_v-1} & \cdots & \lambda_{k'_v-p+1} \\ 1 & 1 & \cdots & 1 \end{bmatrix} \begin{bmatrix} \tilde{t}_1 \\ \tilde{t}_2 \\ \vdots \\ \tilde{t}_p \end{bmatrix} = \begin{bmatrix} \gamma^{\text{old}}_{k'_1} \\ \gamma^{\text{old}}_{k'_2} \\ \vdots \\ \gamma^{\text{old}}_{k'_v} \\ 0 \end{bmatrix}. \tag{15}$$

In general, $(v+1)$ is greater than p, and (15) is an over-determined linear system of equations (OLSE). When $(v+1) = p$, (15) could be solved by the Gaussian elimination algorithm. When $(v+1) > p$, Gauss-Newton method may be used to solve (15) in order to obtain the coefficients of the prediction filter $\tilde{t}$.

3) The Similarity Measurement: After finding the coefficients of the desired prediction filter, the dual lifting step structure of Fig. 4 will form our adaptive wavelet transform. This new transform could be used in the following algorithm for finding the similarity between a reference object data vector and a test image data vector. The signal of interest s (ODV in RASIM) and the test signal x (TDV in RASIM) are assumed to be the input arguments.

A. Offline Steps:

1) Select a non-adaptive wavelet transform, and values of the parameters p and $v \geqslant p-1$.
2) Find the desired prediction filter $\tilde{t}$, as described in Section III.D.2 for s.

B. Online Steps:

1) Apply the non-adaptive and the adaptive lifted wavelet transforms to the test signal x and find the high-pass components γ^{old} and γ.
2) Construct an empty vector D with the same length as γ^{old} and γ.
3) Compare each coefficient of γ^{old} with the corresponding coefficient in γ and if it is decreased, find the vanishing percentage (VP), and save it in vector D

$$D_k = \begin{cases} 0 & |\gamma_k| \geq \left|\gamma^{\text{old}}_k\right| \\ 100 - \left(100\left|\gamma_k/\gamma^{\text{old}}_k\right|\right) & |\gamma_k| < \left|\gamma^{\text{old}}_k\right| \end{cases}, \forall k. \tag{16}$$

4) Sweep vector D with a window of the same length as signal s, and find sum of the VPs for each windowed location, τ

$$\tau_k = \sum_{l=k-L}^{k+L} D_l, \quad \forall k \tag{17}$$

where L is half of total support width of reference signal s and k is the index of elements belonging to the high-pass component. The maximum value for this sum, could be considered as the similarity between reference signal s and test signal x.

4) The Weighted Adaptation in Basic Form: Our experimental results have shown that the above similarity measurement method result in an effective detection algorithm [20]. However, in presence of noise, when the image quality is low (i.e., low signal to noise ratio), the performance of the algorithm would deteriorate. Therefore, a modified version of the prediction filter could help us to boost the detection power in presence of noise by introducing a new weighting parameter in the adaptation process.

If we represent each matrix in (15) by a single letter, we obtain

$$\Lambda \mathbf{T} = \Gamma \tag{18}$$

where Λ is an $(v+1)$-by-p matrix, $\mathbf{T}$ is a column vector with p entries and Γ is a column vector with $(v+1)$ entries.

We desire the vanishing percentage of each coefficient to be proportional to its value, in a way that the larger coefficients

vanish more than the smaller ones. Therefore, a weight vector, $\mathbf{w}$, is added to both sides of (18), resulting in the following weighted OLSE

$$(\mathbf{w} \cdot \times \Lambda)\mathbf{T} = \mathbf{w} \cdot \times \Gamma \tag{19}$$

in which

$$\mathbf{w} = [w_1, w_2, \ldots, w_v, 1]^T \tag{20}$$

where $\cdot\times$ denotes element-by-element product and

$$w_i = 1 + B\frac{\left(\gamma_{k'_i} - \gamma_{k'_v}\right)}{\left(\gamma_{k'_1} - \gamma_{k'_v}\right)}, \quad i = 1, \ldots, v \tag{21}$$

where $\gamma_{k'_1}$ and $\gamma_{k'_v}$ are the largest and the smallest among the selected coefficients, respectively. Therefore, according to (21), weight values will be between one and $(B+1)$. Parameter B is a constant vanishing booster coefficient and its value may vary from one to infinity. The significance of the parameter B is explained in the following section. It is important to note that the Gauss-Newton method may be used to solve (19) in order to obtain the coefficients of the prediction filter $\tilde{t}$.

5) Prediction Filter Design Discussion: Finding the prediction filter for each data vector of the reference template could be a time consuming task. But in many applications, like image retrieval, we only need to compute the prediction filters once, and use the same filters for detecting object of interest in any chosen test image from the database.

Moreover, due to the following reasons, noise or slight deformations in the object of interest, would not have considerable impact on the resulted VPs.

- Most of the large values in the high-pass component remain among large values in the noisy signals as well.
- Both the non-adaptive and the adaptive transforms are applied to the same noisy signal and the vanishing percentage is proportional with the ratio of γ to γ^{old}; therefore the VP values will not experience a considerable change.

There is a trade-off in choosing a value for the parameter B. Greater values for B will result in greater vanishing percentage for larger old high-pass component coefficients, and as a result, the detection algorithm will be less sensitive to the noise, because the large high-pass component coefficients represent edges where the noise has less impact on their values. On the other hand, greater values for B will make it difficult to detect objects that have a large number of small edges.

We conclude that in the noisy images, one may choose larger values for the parameter B to achieve better detection results. Moreover, when a blurred version of the object is expected in the test image, one may choose smaller values for the parameter B. Albeit, even when parameter B is one, the weight vector will keep the vanishing percentage of each coefficient proportional to its value, leading to better detection results in the weighted form of our algorithm.

E. The Whole Matching System

We are using adaptive lifting scheme transform (Section III.D) on the corresponding data vectors from reference template and the test image as the core of our detection algorithm to construct a rotation and scale invariant object detection system. Pseudo log-polar sampling grid, as described in Section III.C, is applied to the properly scaled image patches around each keypoint for acquiring the data vectors. A detailed step-by-step description of RASIM is presented in this section.

1) RASIM, Offline Step: The main building blocks of the offline step are depicted in Fig. 1.

1) The standard SIFT keypoint selection process as described in [16] is applied for finding the reference object template keypoints (OKPs) and assigning proper orientation, scale and location for each keypoint. We call the number of these keypoints, n_{k_O} (Section III.B, Fig. 1(a)).
2) Considering the assigned location, orientation and scale, the image patch around each OKP is taken and the gradient magnitude and the gradient orientation images are computed for them. The pseudo log-polar sampling is applied to the gradient subimages. The set of log-polar pixels which belong to the same ring is taken as a separate reference object data vector(ODV). Therefore, for each of n_{k_O} OKPs, we will acquire n_r ODVs from gradient magnitude subimage and n_r ODVs from gradient orientation subimage. The length of each data vector will be equal to the number of log-polar pixels in angular direction, n_θ (Section III.C, Fig. 1(b)).
3) The adaptive wavelet transform is designed for each of $n_{k_O} \times 2 \times n_r$ ODVs, as described in Section III.D (Fig. 1(c)). The length of lifting step filter (p) and the number of large values in the high-pass component (v) are two main fixed parameters in this step. The prediction filters, $P_{i,r}$, for $i = 0, \ldots, n_{k_O} - 1$ and $r = 1, \ldots, (2 \times n_r)$ are saved to be used for the matching process in the online step.

2) RASIM, Online Step: The main building blocks of the online step are depicted in Fig. 2. The process which is shown in this figure, shows how we find the similarity between any pair of keypoints from the reference template and the test image.

1) The standard SIFT keypoint selection process is applied for finding the test image keypoints (TKPs) and assigning proper orientation, scale and location for each keypoint. We call the number of these keypoints, n_{k_T} (Section III.B, Fig. 2(a)).
2) Considering the assigned location, orientation and scale, the image patch around each TKP is taken and the gradient magnitude and the gradient orientation images are computed for them. The pseudo log-polar sampling is applied to the gradient subimages. The set of log-polar pixels which belong to the same ring is taken as a separate test image data vector (TDV). Therefore, for each of n_{k_T} TKPs, we will acquire n_r TDVs from gradient magnitude subimage and n_r TDVs from gradient orientation subimage. The length of each data vector will be equal to the number of log-polar pixels in angular direction, n_θ (Section III.C, Fig. 2(b)).
3) The core detection algorithm will be used to find the similarity between $\mathrm{TDV}_{j,r}$ and $\mathrm{ODV}_{i,r}$. $\mathrm{TDV}_{j,r}$ is the data vector of jth test image keypoint at ring r. $\mathrm{ODV}_{i,r}$ is the data vector of ith reference object keypoint at ring r. The adaptive transform will be constructed using the pre-

diction filter $P_{i,r}$, which we have saved for $\mathrm{ODV}_{i,r}$ in the offline step. Both of the non-adaptive wavelet transform and the designed adaptive transform are applied to $\mathrm{TDV}_{j,r}$ and wavelet domain coefficients are compared as described in Section III.D to find the similarity value $\rho_{i,j,r}$. This step will be repeated for $i = 0, \ldots, n_{k_O} - 1$, $j = 0, \ldots, n_{k_T} - 1$, and $r = 1, \ldots, (2 \times n_r)$.

4) Similarity between keypoint pairs will be equal to the Gaussian weighted sum of similarity between their data vectors. We use (22) to find similarity between ith reference object keypoint, OKP_i and jth test image keypoint, TKP_j

$$\sum_{r=1}^{2\times n_r} w_r \rho_{i,j,r} \tag{22}$$

where

$$w_r = e^{-((r-1) \bmod n_r)^2 / n_r^2}. \tag{23}$$

Operation "mod" stands for modulus after division. The best candidate match for each OKP in the database of test image keypoints is the one which will result in the maximum similarity value.

Similar to the SIFT keypoint matching, we discard a match for an OKP by comparing the similarity value of the best match to that of the second-best match. We reject all matches in which the distance to "best" over distance to "second best" ratio is greater than 0.8. This measure performs well because correct matches need to have the maximum similarity value significantly larger than the best incorrect match to achieve reliable matching [1]. The reference object detection proceeds by a Hough transform to identify clusters that agree on a single object pose and performing verification through least-squares solution for consistent pose parameters.

IV. Implementation Notes and Experimental Results

A. Discussion and Implementation Notes

The first advantage of using each ring in the pseudo log-polar sampling grid as input data vectors is because the wrong rotation assignment to a keypoint will only result in a circular shift in the data vector. On the other hand both the adaptive and non-adaptive wavelet transforms are translation invariant. This will help to reduce the effect of wrong rotation assignment to a keypoint, in degrading the similarity value.

Another advantage of log-polar mapping for interest point matching comes from its space variant sampling property. It provides means to have high resolution in the areas of interest and also to control the number of information bearing pixels (length of each data vector). The number of data vectors is controlled by the number of rings n_r and the number of samples in each data vector is controlled by the number of receptive fields in angular direction n_θ. The sampling resolution of log-polar mapping is higher around fovea and decreases exponentially as it gets further from that, so the area near to center point (keypoint location) automatically becomes more important than the surrounding areas which are more likely to be the background of the target image.

TABLE I
Typical Settings Used for Presenting the Average Computational Time

n_r	16
n_θ	64
Non-adaptive wavelet transform	Bior2.2
The length of lifting step filter (p)	16
# large values in the high-pass component (v)	24

Most of the time consuming tasks in RASIM can be done in the offline step. The LUT initialization for log-polar mapping and designing lifting step filter for adaptive wavelet transform are required to be done only once for the given reference template in the offline step. Computational time for MATLAB implementation of RASIM on the Pentium 2.8 GHz personal computer is approximately 4 milliseconds, for finding similarity value of a pair of keypoints. This time includes preparing of OKP and TKP data vectors, designing adaptive transform for OKP data vectors, applying non-adaptive and adaptive transform to TKP data vectors and comparing wavelet domain coefficients. This is calculated based on the average runtime of our experiments for the typical settings presented in Table I. A processing time comparison of SIFT, Speeded-Up Robust Features (SURF) [17] and RASIM is also presented at the end of Section IV.B.

The most time consuming task at the online step is log-polar mapping. Our experiments show that in average nearly 80% of the total online execution time is occupied by LUT based log-polar mapping. It is due to the software implementation of log-polar mapping in our experiments. The runtime of the object detection system can considerably be improved using the hardware implementation for the log-polar mapping. Albeit the true log-polar sensors have already been built [26], [27].

The best choices for the value of parameters p and v can be determined experimentally by studying different range of values under various realistic simulations. Our experiments show that the correct detection percentage of RASIM provides the most reliable results in $n_\theta = 64$ data vectors when the value of parameter p is between 12 and 21 and the value of parameter v is between 20 and 32. Within these range of values the correct detection percentage did not show considerable increase or decrease. Therefore, we have selected the typical values of 16 and 24 for the parameters p and v, respectively.

B. Keypoint Matching Evaluation

Due to page limit, we have excluded the experimental results of the core detection algorithm (Section III.D) on data vectors. Sample experimental results of the core detection algorithm on 1D signals may be found in our previously published papers [20] and [24].

The performance of keypoint descriptor matching is evaluated by descriptor repeatability measurement as it is used in the widely accepted framework of [28]. Based on this framework, the repeatability scores for each keypoint descriptor are evaluated on the *boat* and *graffiti* sequences of Fig. 5 which are available from [29].

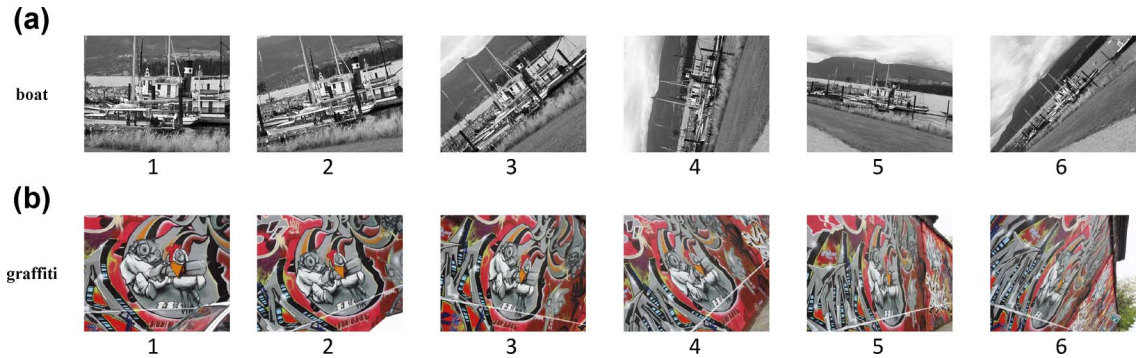

Fig. 5. Keypoint matching evaluation test images. (a) *boat* sequence which includes scale changed and rotated images, (b) *graffiti* sequence which includes viewpoint changed images.

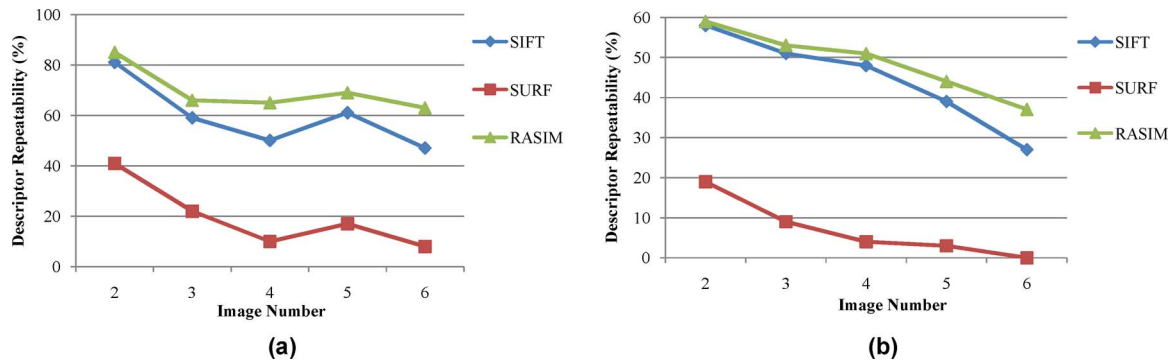

Fig. 6. Descriptor repeatability of SIFT, SURF and RASIM between first image and other five images of test sequences. (a) *boat* sequence (rotation and zoom), (b) *graffiti* sequence (viewpoint).

The descriptor repeatability measurement of two images I1 and I2 is computed as the ratio between the number of point-to-point correspondences that can be established for detected points by the keypoint matching algorithm and the mean number of keypoints detected in two images [30]

$$r_{1,2} = \frac{C(I_1, I_2)}{\text{mean}(m_1, m_2)} \tag{24}$$

where $C(I_1, I_2)$ denotes the number of corresponding couples, m_1 and m_2 are the number of detected keypoints in I_1 and I_2, respectively. Two points correspond if the error in relative location does not exceed 1.5 pixel in the coarse resolution image and the ratio of detected scales for these points does not differ from the real scale ratio by more than 20%.

The *boat* sequence is challenging because of large changes in rotation and zoom. Fig. 6(a) shows the descriptor repeatability of SIFT, SURF and RASIM between first image and other five images in this sequence. The results show that, when the scale change and rotation angle gets larger, RASIM performs better than SIFT and SURF.

The *graffiti* sequence is to evaluate stability of these methods when we have affine transformations. Being robust to viewpoint changes is important in panorama stitching. Descriptor repeatability diagrams of the same three methods for this sequence are shown in Fig. 6(b). RASIM and SIFT have almost equal repeatability score when the viewpoint change is small, but for the large viewpoint changes, RASIM performs slightly better than SIFT. SURF finds the least matched keypoints and doesn't work well when we have large rotation or large viewpoint change.

TABLE II
PROCESSING TIME COMPARISON OF SIFT, SURF, AND RASIM (MATLAB IMPLEMENTATIONS). EACH LINE SHOWS THE AVERAGE PROCESSING TIME OF MATCHING TWO IMAGES IN THE GIVEN TEST SEQUENCE

Test sequence	SIFT	SURF	RASIM
boat	48.1 (sec)	5.1 (sec)	53.6 (sec)
graffiti	45.2 (sec)	4.7 (sec)	49.3 (sec)

There was other data sets from [29] which were including image sequences with illumination changes and blurred images. Our experiments show that for those sequences RASIM and SIFT had similar descriptor repeatability scores and are not illustrated in this paper.

The processing time of SIFT, SURF and RASIM are evaluated for the *boat* and *graffiti* datasets. This evaluation is mainly influenced by the input parameters of the three algorithms. We have chosen the parameters of SIFT and SURF algorithms according to the original papers [1], [17]. The typical settings presented in Table I were used as the input parameters of RASIM. This time includes the whole process of detecting keypoints, calculating descriptors and matching the keypoints in the MATLAB implementation of these algorithms. First image of each sequence is matched with other five images of the test sequence to calculate the average processing time of matching two images. The results are presented in Table II which shows that SURF is much faster than SIFT and RASIM. Although RASIM is slightly slower than SIFT, but is superior

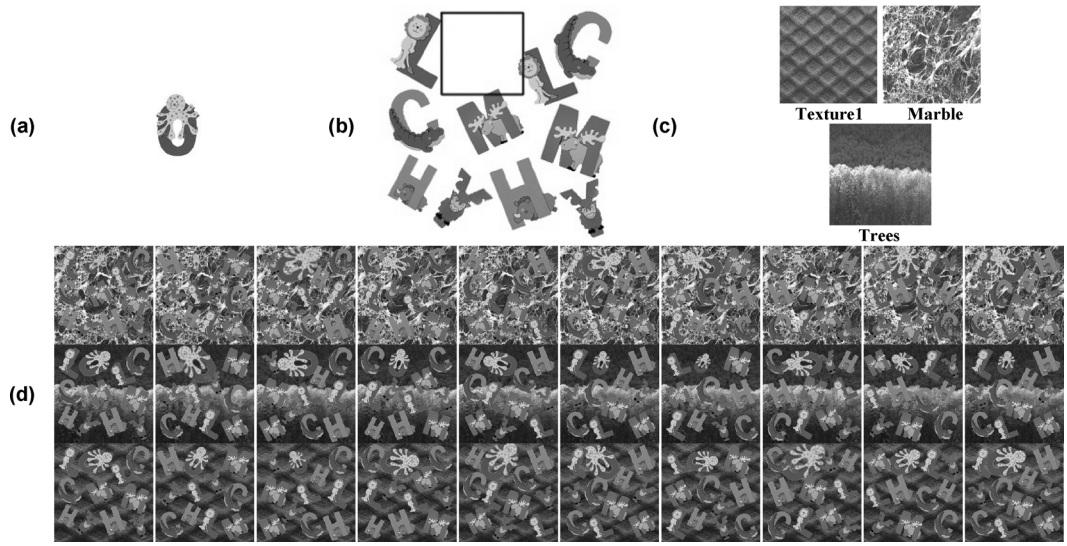

Fig. 7. RASIM evaluation example, (a) Reference template, (b) Sample test image configuration, (c) Three different background images (Texture1, Marble, and Trees), (d) 30 different test images after adding backgrounds and toy letter "O".

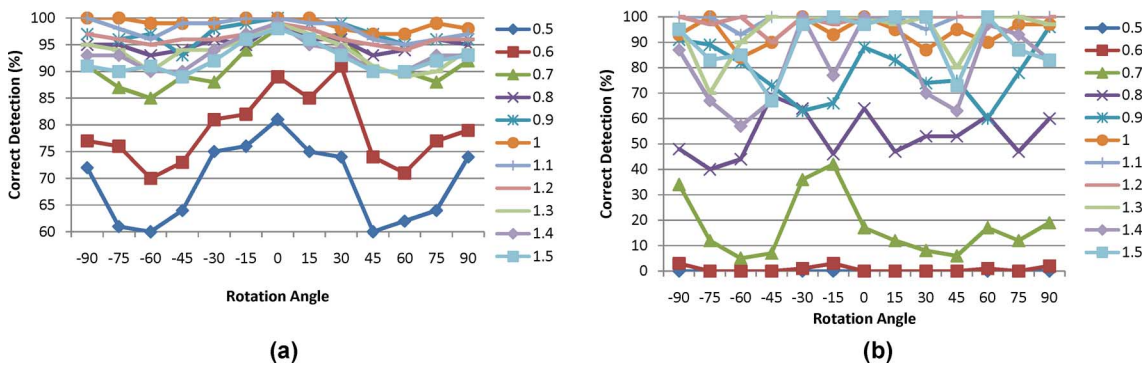

Fig. 8. Correct detection percentage evaluation results. Each point is the correct detection percentage obtained by $6 \times 30 = 180$ different tests for a fixed rotation angle from -90° to $+90^\circ$ and scaling factor from 0.5 to 1.5, (a) RASIM, (b) SIFT.

in terms of keypoint matching quality. As we have mentioned earlier, the runtime of RASIM can considerably be improved using the hardware implementation for the log-polar mapping.

C. Image Matching Evaluation

We have conducted a comprehensive set of experiments to obtain a detailed evaluation for the results of RASIM. We have created a large number of test images with different configuration of the toy letters. For evaluation, we select a toy letter as the reference template and create 30 different test images as follows. For example, the toy letter "O" which is shown in Fig. 7(a), is selected as the reference template. We select 10 different test images similar to the one presented in Fig. 7(b). Each test image includes different configuration of the toy letters. A sample test image is created by placing rotated and scaled form of the reference template instead of the empty black box in Fig. 7(b) and adding one of the three different background images (Texture1, Marble, Trees) shown in Fig. 7(c). The resulting test images are illustrated in Fig. 7(d). We have conducted our experiments using 6 different toy letters (C, H, L, M, O, Y) as the reference templates.

Rotation angle range of the reference template instance in the test images was chosen from -90° to 90° with 15° increments (13 different rotation angles). Scaling factor range of the reference template instance in the test images was set from 0.5 to 1.5 with 0.1 steps (11 different scaling factors). Considering 10 different configuration for basic toy letter test images, 3 different background images, 13 different rotation angles and 11 different scaling factors for the reference template instance, this experiment consists of 4290 different test images for a toy letter. From another point of view, for each combination of values in the chosen range of rotation angles and scaling factors, we conducted 30 different tests.

RASIM is used to locate the reference template in each test image. The typical settings presented in Table I were used in this experiment. Correct detection percentages obtained by a total of 6×4290 tests are illustrated in Fig. 8(a) for the proposed object detection system and in Fig. 8(b) for SIFT. Each point in this figure represents the correct detection percentage obtained by 6×30 different tests for a fixed rotation angle from -90° to $+90^\circ$ and scaling factor from 0.5 to 1.5. Excluding the boundary results obtained in scales 0.5 and 0.6, the correct detection rate is above 85%. Our experiments show that the proposed detection

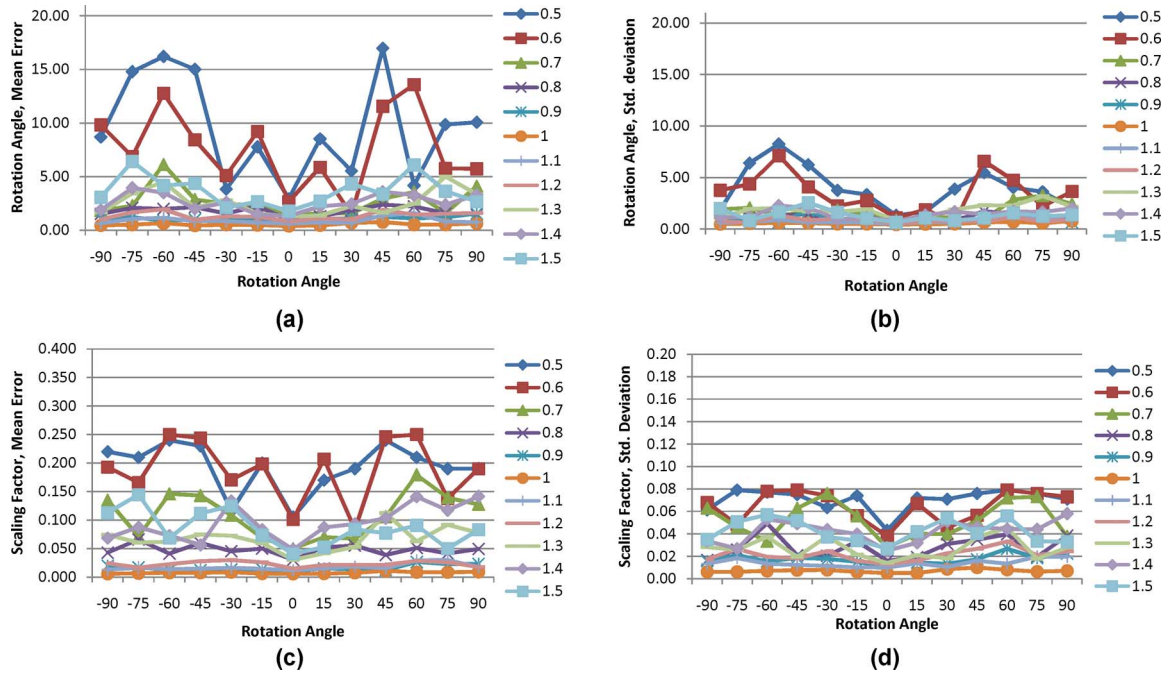

Fig. 9. Mean error and standard deviation for the estimated rotation angle and scaling factor in the whole tests. (a) Mean error of the estimated rotation angles. (b) Standard deviation of the estimated rotation angles. (c) Mean error of the estimated scaling factors. (d) Standard deviation of the estimated scaling factors.

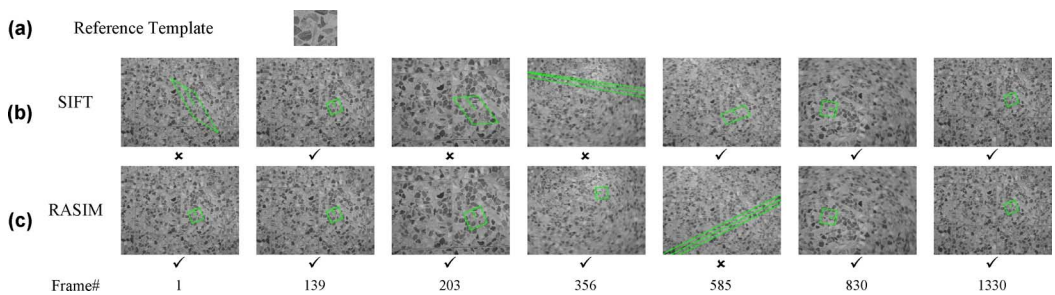

Fig. 10. Floor tile pattern #1 detection example, (a) Reference template, (b) Sample results of SIFT (Correct detection: 84%), (c) Sample results of RASIM (Correct detection: 91%).

system is more accurate than SIFT. RASIM is more accurate than SIFT specially when the scaling factor is under 0.7 and above 1.3.

We have conducted this comparison, as SIFT is the widely accepted benchmark method for object detection in the literature. Although SURF is superior to SIFT in terms of runtime efficiency, but as the feature point selection and object detection quality is our main concern in this paper, we have chosen SIFT instead of SURF. Comparing SIFT against SURF, it is already shown that SIFT performs best in terms of keypoint match ratio and total number of correct keypoint matches [31]. keypoints in SURF are found by using a so called fast-hessian detector that bases on an approximation of the hessian matrix for a given image point. We may incorporate fast keypoint detection approach of SURF instead of SIFT like keypoint detection step in RASIM to further improve the computational time. The scale-invariant center-surround detector (CenSurE) is also superior to SIFT and SURF in terms of runtime efficiency, but is not fully rotation invariant and is relatively sensitive to in-plane rotations [18].

The estimated rotation angle and scaling factor obtained for each test image are compared with the true rotation angle and scaling factor of the reference template instance in the test image. Mean error and standard deviation for the estimated rotation angle and scaling factor in the whole 6×4290 tests are illustrated in Fig. 9(a) through (d). The overall performance is rather good as in the majority of tests the mean error of the estimated rotation angle is less than 11° and the mean error of the estimated scaling factor is less than 0.15.

D. Detection Examples

Fig. 10 shows sample examples of object detection in a video. We have recorded the video from floor tile patterns by moving around the camera so that we may capture various pattern distortions in video frames, including rotation, scaling, blurring, change of view point and illumination changes. The reference template is a clip of a tile pattern (of size 300 by 246 pixels) which is shown in Fig. 10(a). SIFT and RASIM are used to detect the reference pattern clip in all 1330 video frames (of size 640 by 480 pixels).

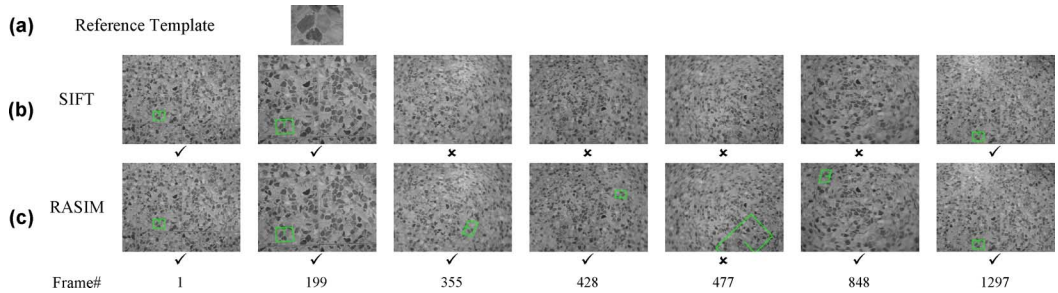

Fig. 11. Floor tile pattern #2 detection example, (a) Reference template, (b) Sample results of SIFT (Correct detection: 76%), (c) Sample results of RASIM (Correct detection: 88%).

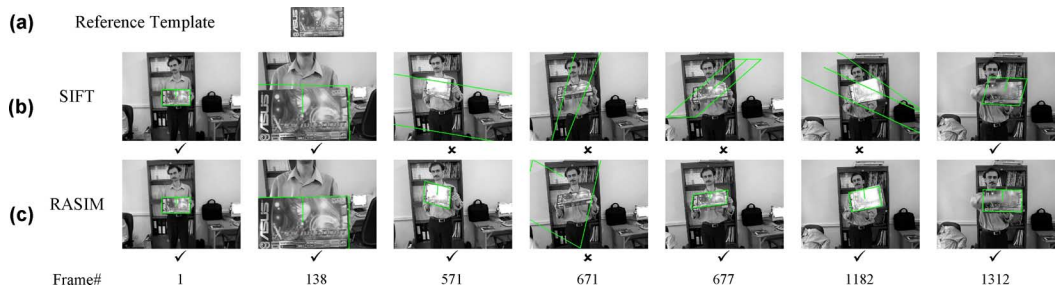

Fig. 12. Graphic card box detection example, (a) Reference template, (b) Sample results of SIFT (Correct detection: 87%), (c) Sample results of RASIM (Correct detection: 92%).

The performance of object detection is evaluated by the *overlap error* measurement as it is defined and used in the widely accepted framework of [28]. The ground truth bounding box of the object of interest in each frame is determined by the human-marked data. Two regions are considered as a correct match if the overlap error, defined as the error in the image area covered by the regions, is sufficiently small. Similar to [28], the overlap error threshold is fixed to 40% in all the experiments.

The detection results in sample frames are illustrated in Fig. 10(b) for SIFT and in Fig. 10(c) for RASIM. This reference pattern clip was mostly subject to rotation and scaling in the video frames, although blurring and slight changes of view point were in effect too. Correct detection percentage of RASIM is nearly 7% more than SIFT in this example.

Fig. 11 shows sample examples of a more challenging object detection. In this example we have selected 259 by 197 pixels pattern clip shown in Fig. 11(a) as the reference template which is subject to severe blurring and distortions in most of the video frames. In some of the video frames blurring, change of view point and illumination changes have simultaneously occurred (e.g., Frame #848 which is shown in Fig. 11). The detection results in sample frames are illustrated in Fig. 11(b) for SIFT and in Fig. 11(c) for RASIM. The correct detection percentage of both methods are decreased. Yet, this time the correct detection percentage of RASIM is nearly 12% more than SIFT which demonstrates the higher performance of RASIM when various object distortions may simultaneously occure in the given test images.

Fig. 12 shows another object detection example where mostly change of view point, occlusion and spot illuminations over reference template are considered. Graphic card box image of size 537 by 302 pixels shown in Fig. 12(a) is selected as the reference template. The detection results in sample frames (of size 640 by 480 pixels) are illustrated in Fig. 12(b) for SIFT and in Fig. 12(c) for RASIM. Within the frames where the object of interest is occluded (e.g., frame #1312) both SIFT and RASIM perform well. While in change of view point cases like frame #677 and spot illuminations like frame #571, RASIM has been more effective than SIFT. The complete video results of Figs. 10, 11, and 12 are available at http://www.dml.ir/rasim/.

V. Conclusion

In this paper, we have presented a novel adaptive lifted wavelet transform based algorithm for matching image interest points between a reference template and a given test image. The evaluation results show that RASIM interest point matching algorithm provides efficient distinctiveness to detect an object of interest in the test images.

The most time consuming tasks have been moved to the offline steps of the algorithm, therefore for the several thousand keypoints that can be extracted from a typical image the online steps can be executed with near real-time performance on standard PC hardware. Also, the computation time can be improved using hardware implementation for the log-polar mapping.

Many variations of RASIM could be designed to improve its performance. For example, here we have only focused on grayscale images. The color components may be considered in the future developments. Also, here we have only used "gradient magnitude" and "gradient orientation" to provide two types of input data vectors. Other image feature extractors may be included as the preprocessing steps for providing more input data vectors.

RASIM may be used as the basic building block of any application that require identification of matching interest points between images. In this paper we have focused on the object detection application. Other potential applications

include image panorama assembly, moving object tracking, image segmentation, view matching for 3D reconstruction and robot localization.

REFERENCES

[1] D. G. Lowe, "Distinctive image features from scale-invariant keypoints," *Int. J. Comp. Vis.*, vol. 60, no. 2, pp. 91–110, Nov. 2004.

[2] C. Rotaru, J. Schipritt, T. Graf, J. Zhang, and W. P. Buchwald, "High accuracy object detection and following in color images for automotive applications," in *Proc. IEEE Int. Conf. Inf. Acquisition*, Macau, Hong Kong, China, 2005, pp. 570–575.

[3] A. Price, J. Pyke, D. Ashiri, and T. Cornall, "Real time object detection for an unmanned aerial vehicle using an fpga based vision system," in *Proc. IEEE Int. Conf. Robotics Autom.*, Orlando, FL, USA, May 15–19, 2006, pp. 2854–2859.

[4] S.-C. Cheng, "Visual pattern matching in motion estimation for object-based very low bit-rate coding using moment-preserving edge detection," *IEEE Trans. Multimedia*, vol. 7, no. 2, pp. 189–200, Apr. 2005.

[5] S. Hutchinson, G. Hager, and P. Corke, "A tutorial on visual servo control," *IEEE Trans. Robotics Autom.*, vol. 12, no. 5, pp. 651–670, Oct. 1996.

[6] Y. Bentoutou, N. Taleb, K. Kpalma, and J. Ronsin, "An automatic image registration for applications in remote sensing," *IEEE Trans. Geosci. Remote Sens.*, vol. 43, no. 9, pp. 2127–2137, Sep. 2005.

[7] L. G. Brown, "A survey of image registration techniques," *ACM Comp. Surv.*, vol. 24, no. 4, pp. 325–376, Oct. 1992.

[8] H. Peng, F. Long, and Z. Chi, "Document image recognition based on template matching of component block projections," *IEEE Trans. Pattern Anal. Mach. Intell.*, vol. 25, no. 9, pp. 1188–1192, Sep. 2003.

[9] R. M. Dufour, E. L. Miller, and N. P. Galatsanos, "Template matching based object recognition with unknown geometric parameters," *IEEE Trans. Image Process.*, vol. 11, no. 12, pp. 1385–1396, Dec. 2002.

[10] L. D. Stefano, M. Marchionni, and S. Mattoccia, "A fast area-based stereo matching algorithm," *Image Vis. Comput.*, vol. 22, no. 12, pp. 983–1005, Oct. 2004.

[11] A. D. Bimbo and P. Pala, "Visual image retrieval by elastic matching of user sketches," *IEEE Trans. Pattern Anal. Mach. Intell.*, vol. 19, no. 2, pp. 121–132, Feb. 1997.

[12] M. Ferreira, S. Kiranyaz, and M. Gabbouj, "Multi-scale edge detection and object extraction for image retrieval," in *Proc. IEEE Int. Conf. Acoustics, Speech, Signal Process.*, Toulouse, France, May 14–19, 2006, pp. II-381–II-384.

[13] M. Amiri and H. R. Rabiee, "A novel rotation/scale invariant template matching algorithm using weighted adaptive lifting scheme transform," *Pattern Recognit.*, vol. 43, no. 7, pp. 2485–2496, Jul. 2010.

[14] K. Mikolajczyk and C. Schmid, "Scale and affine invariant interest point detectors," *Int. J. Comp. Vis.*, vol. 60, no. 1, pp. 63–86, Oct. 2004.

[15] Y. Ke and R. Sukthankar, "Pca-sift: A more distinctive representation for local image descriptors," in *Proc. IEEE Computer Vis. Pattern Recognit.*, Washington, DC, 2004, pp. 506–513.

[16] D. G. Lowe, "Object recognition from local scale-invariant features," in *Proc. IEEE Int. Conf. Comput. r Vis.*, Kerkyra, Greece, Sep. 1999, pp. 1150–1157.

[17] H. Bay, A. Ess, T. Tuytelaars, and L. V. Gool, "Speeded-up robust features (surf)," *Comput. Vis. Image Understand.*, vol. 110, no. 3, pp. 346–359, Jun. 2008.

[18] M. Agrawal, K. Konolige, and M. R. Blas, "Censure: Center surround extremas for realtime feature detection and matching," in *Proc. 10th Eur. Conf. Comput. Vis*, Marseille, France, Oct. 2008, pp. 102–115.

[19] T. Tuytelaars and K. Mikolajczyk, "Local invariant feature detectors: A survey," *Found. Trends Comput. Graph. Vis.*, vol. 3, no. 3, pp. 177–280, 2008.

[20] M. Amiri and H. R. Rabiee, "A new adaptive lifting scheme transform for robust object detection," in *Proc. IEEE Int. Conf. Acoust., Speech, Signal Process.*, Toulouse, France, May 2006, pp. II: 749–752.

[21] E. L. Schwartz, "Computational anatomy and functional architecture of striate cortex: A spatial mapping approach to perceptual coding," *Vis. Res.*, vol. 20, pp. 645–669, 1980.

[22] J. Traver, "Motion estimation algorithms in log-polar images and application to monocular active tracking," Ph.D. dissertation, Departament de Llenguatges i Sistemes Informatics, Universitat Jaume I, Jaume, Spain, 2002.

[23] M. Tistarelli and G. Sandini, "Dynamic aspects in active vision," *CVGIP: Image Understand.*, vol. 56, no. 1, pp. 108–129, Jul. 1992.

[24] M. Amiri and H. R. Rabiee, "Object detection based on weighted adaptive prediction in lifting scheme transform," in *Proc. IEEE Int. Symp. Multimedia*, San Diego, CA, Dec. 11–13, 2006, pp. 652–656.

[25] I. Daubechies and W. Sweldens, "Factoring wavelet transforms into lifting steps," *J. Fourier Anal. Appl.*, vol. 4, no. 3, pp. 247–269, 1998.

[26] R. Wodnicki, G. W. Roberts, and M. Levine, "Design and evaluation of a log-polar image sensor fabricated using a standard 1.2 um asic cmos process," *IEEE J. Solid-State Circuits*, vol. 32, no. 8, pp. 1274–1277, Aug. 1997.

[27] R. Etienne-Cummings, J. V. der Spiegel, P. Mueller, and M. Z. Zhang, "A foveated silicon retina for two-dimensional tracking," *IEEE Trans. Circuits Syst. II-Analog Digit. Signal Process.*, vol. 47, no. 6, pp. 504–517, Jun. 2000.

[28] K. Mikolajczyk, T. Tuytelaars, C. Schmid, A. Zisserman, J. Matas, F. Schaffalitzky, T. Kadir, and L. V. Gool, "A comparison of affine region detectors," *Int. J. Comp. Vis.*, vol. 65, no. 1–2, pp. 43–72, Nov. 2005.

[29] A. Zisserman, Visual Geometry Group Website Aug. 2010 [Online]. Available: http://www.robots.ox.ac.uk/vgg/data/data-aff.html, Address: Last Access time:

[30] K. Mikolajczyk and C. Schmid, "Indexing based on scale invariant interest points," in *Proc. IEEE Int. Conf. Comput. Vis.*, Vancouver, BC, Canada, Jul. 2001, pp. 525–531.

[31] J. Bauer, N. Snderhauf, and P. Protzel, "Comparing several implementations of two recently published feature detectors," presented at the IFAC Symp. Intell. Autonomous Vehicles, Toulouse, France, Sep. 2007.

Mahdi Amiri received the B.Sc. degree in electrical engineering from University of Tabriz, Tabriz, Iran, in 1997, and the M.Sc. and Ph.D. degrees in computer engineering from Sharif University of Technology, Tehran, Iran in 2003 and 2010, respectively.

He is a member of Sharif University's Advanced Information and Communication Technology Research Center (AICTC). His current research interests include adaptive signal processing, wavelet theory, lifting scheme and object detection.

Hamid R. Rabiee (SM'07) received the B.S. and M.S. degrees (with Great Distinction) in electrical engineering from CSULB, in 1987 and 1989, respectively, the E.E.E. degree in electrical and computer engineering from University of Southern California, and the Ph.D. degree in electrical and computer engineering from Purdue University, West Lafayette, IN, in 1996.

From 1993 to 1996 he was a Member of Technical Staff at AT&T Bell Laboratories (Lucent), Indianapolis, IN. From 1996 to 1999 he worked as a Senior Software Engineer at Intel Corporation. He was also with PSU and OGI Universities as an Adjunct Professor of Electrical and Computer Engineering from 1996 to 2000. Since September 2000, he has been with Sharif University of Technology (SUT), Tehran, Iran. He is the founder of Sharif University's Advanced Information and Communication Technology Research Center (AICTC), Advanced Technologies Incubator (SATI), Digital Media Laboratory (DML), and Mobile Value Added Services laboratory (M-VASL). He is currently the Director of AICTC and a faculty member at the department of Computer Engineering at SUT. His research interests include multi-resolution image & video processing, machine learning, multimedia systems, complex networks, and multimedia overlay/P2P networks.

Prof. Rabiee has received numerous awards and honors for his scientific, academic and industrial contributions and holds two U.S. patents.